Involvement of Various Molecular Events in Cellular Injury Induced by Smokeless Tobacco

ARTICLE *in* CHEMICAL RESEARCH IN TOXICOLOGY · JULY 2010

Impact Factor: 3.53 · DOI: 10.1021/tx900458x · Source: PubMed

Involvement of Various Molecular Events in Cellular Injury Induced by Smokeless Tobacco

Pramod K. Avti,[†] Kim Vaiphei,[‡] Chander M. Pathak,[†] and Krishan L. Khanduja*,[†]

Departments of Biophysics and Histopathology, Postgraduate Institute of Medical Education and Research, Chandigarh 160012, India

Received December 28, 2009

Smokeless tobacco (ST) consumption is implicated in the pathogenesis of oral diseases, including cancer. However, its pathological effect in other organs is not well understood. In the present study, the effect of aqueous extract of smokeless tobacco (AEST) prepared from "gutkha" (a form of ST) on the xenobiotic drug-metabolizing enzymes, histopathological changes, and damage to the genetic material in lung, liver, and kidney of rats was evaluated. Animals were orally administered AEST at a low dose (L-AEST, 96 mg/kg body wt/day) for 2 (L-AEST$_2$) and 28 weeks (L-AEST$_{28}$) and at a high dose (H-AEST, 960 mg/kg body wt/day) for 2 weeks (H-AEST$_2$). Real-time PCR and immunohistological studies showed that administration of L-AEST$_2$ did not induce the expression of phase I cytochrome P450s (CYP1A1, 1A2, and 2E1) and phase II μ-glutathione-s-transferase (GST-μ) drug-metabolizing enzymes in lung, liver, and kidney. Although H-AEST$_2$ administration significantly induced both gene and protein expression of CYP1A1, 1A2, and 2E1 in all of the above organs, it mildly expressed the phase II detoxifying enzyme, GST-μ, in type I and type II epithelial cells of lung and in proximal tubular cells of kidney. L-AEST$_{28}$ enhanced the gene and protein expression of CYP1A1, 1A2, and 2E1 in lung, liver, and kidney in a differential manner and induced the expression of GST-μ in lung and kidney. L-AEST$_{28}$ induced the micronuclei formation in the peripheral blood mononuclear cells, TNF-α in plasma, and myeloperoxidase activity in the organs. L-AEST$_{28}$ significantly enhanced Bax, p53, and NF-κB and decreased Bcl-2 gene expressions differentially in an organ-specific manner. The differential changes in these organs due to AEST might be due to their different physiological functions and variable sensitivities toward the metabolites of AEST, which create a microenvironment favorable for AEST-induced pathogenesis. This study broadens the insight into the different molecular mechanisms in various organs, which appear to be deregulated due to AEST. Understanding these processes may help in clinical treatment planning strategies for tobacco-related diseases.

Introduction

Smokeless tobacco (ST) is a very broad term that refers to more than 30 different types of products. It is also called spit tobacco or chewing tobacco. These products are used around the world but are most common in Northern Africa, Southeast Asia, and the Mediterranean region (*1, 2*). Most of the users seem to be unaware of the harmful health effects and, therefore, use ST to "treat" toothaches, headaches, and stomachaches. This false impression only promotes tobacco use among youth. The use of ST and its new products is increasing not only among men but also among children, teenagers, women, and immigrants of South Asian origin and medical and dental students (*3, 4*).

The cytochrome P450 (CYP) enzymes are a multigene superfamily of monooxygenase hemeproteins of the microsomal mixed function oxidase system that is central to the activation and detoxification of carcinogens, other toxic chemicals including tobacco products, drugs, pesticides, and organic pollutants and to the metabolism of a wide array of endogenous substances (*5*). The CYP1A family comprises two proteins, CYP1A1 and 1A2 (involved in the metabolism of aromatic hydrocarbons), and CYP2E consists of CYP2E1 (responsible for metabolism of carcinogenic *N*-nitrosoamines) that play important roles in carcinogen activation, and glutathione-s-transferases are involved in xenobiotic detoxification (*6*). Like CYP1A1 and CYP1A2, CYP1B1 is also involved for the metabolism of polycyclic aromatic hydrocarbons in liver, lung, and other organs. Wide substrate specificity of CYP is due to the existence of numerous forms that are regulated independently. The progression of toxicities and carcinogenicities due to ST is facilitated by CYP-mediated bioactivation. In general, metabolites produced by phase I enzymes are detoxified by phase II enzymes and excreted into urine and/or bile. Drug-metabolizing enzymes convert many tobacco carcinogens into DNA-binding metabolites in different organs and can thereby modulate intermediate effect markers such as DNA adducts and, ultimately, the risk for cancer.

The mixture of ST is chewed slowly, and in this process, the aqueous extract due to saliva is not only absorbed locally but also ingested and enters into the systemic circulation. Cells of different organs respond to the continuous exposure to potentially toxic xenobiotics by the induction of xenobiotic-metabolizing enzymes. While the liver has been recognized as the major site of drug or xenobiotic (foreign compound) metabolism; recently, much attention has also been paid to the metabolism of xenobiotics by extra hepatic tissues, in particular, at portals of entry into the body (i.e., the lung, intestine, and skin), which is markedly influenced by the xenobiotics (*7*) and the excretory organs such as kidney to eliminate them from the

* To whom correspondence should be addressed. Tel: +91-172-2755246. Fax: +91-172-2744401. E-mail: klkhanduja@gmail.com.
[†] Department of Biophysics.
[‡] Department of Histopathology.

10.1021/tx900458x
Published on Web 06/03/2010

body (*8*). In most cases, in vitro enzymatic activities of liver are significantly higher than those of lung, but these differences may be offset in vivo by other factors such as blood flow and distribution of xenobiotics in an organ (*9*). Thus, for the compounds that are concentrated in lung, liver, and kidney tissue (*10, 11*), the contribution by these organs to the overall metabolism of the xenobiotics may be far greater than can be determined from in vitro enzymatic activities. However, with some important compounds, qualitative and quantitative differences are found in the metabolites formed and the inducibility of the enzymes in different organs. The intracellular distribution of different metabolic isozymes may play a key role in determining the fate of cellular specificity of some toxins and their metabolites in various organs.

The use of "gutkha" has been classified as carcinogenic to humans and may be associated with oral disease (*12*−*14*). Several oral lesions are associated with ST use, of which oral cancer is the most prominent. Its use can be addictive, leading to oral leukoplakias (oral mucosal lesions) and gingival recession and may play a contributory role in the development of cardiovascular disease, peripheral vascular disease, hypertension, peptic ulcers, and fetal morbidity and mortality (*15*). Epidemiologic studies have shown a correlation between use of ST and adverse health outcomes manifested as an increased incidence of cardiovascular, renal, and respiratory diseases (*16*). Although interest is growing in the patterns, distribution, consumptions, and compositions of tobacco and its use in various parts of the world (*17*), the precise health effects of ST use are uncertain and may not necessarily be limited to oral cancers (*18*), as it has been recently reported by us that AEST induces inflammation in liver and lung (*19*).

Given the great number of carcinogen-activating and detoxifying enzymes, the variation in their expression in different organs, and the complexity of exposures to tobacco carcinogens, assessment of a single polymorphic enzyme may not be sufficient to assess their role in carcinogenesis. The events occurring during the process of metabolizing enzyme induction have been studied extensively, but relatively little is known regarding the short- and long-term effects of ST-induced xenobiotic enzymes and their implications in various organs. However, to the best of our knowledge, no study has been reported so far that demonstrates the induction of various metabolic enzymes and the expressions of cell survival genes by the ST in different organs. The present study, therefore, was designed to evaluate the effects of short- and long-term use of the aqueous extract of "gutkha" on the xenobiotic enzymes (CYP) activation, genetic damage, and the expression of apoptotic/antiapoptotic genes in male Wistar rats.

Materials and Methods

Materials. 3,3′-Diaminobenzidine tetrahydrochloride (DAB), acridine orange (AO), citric acid, hexadecyl trimethylammonium bromide buffer (HTAB), methanol, *o*-dianisidine dihydrochloride, triton X-100, and xylene were purchased from Sigma Chemicals (St. Louis, MO). Rat TNF-α ELISA Kit was obtained from M/s Diaclone (France). Rat-antirabbit primary antibody of CYPs (CYP1A1, CYP1A2, and CYP2E1), μ-glutathione-s-transferase (GST-μ), and horseradish peroxidase (HRP)-labeled secondary antibodies were obtained from M/s Chemicon International (United States). Phosphate-buffered saline (PBS), Tris-HCl buffer, and ethylenediamine tetrachloroacetic acid (EDTA) were purchased from M/s HiMedia Chemicals (Mumbai, India). The pellet diet was obtained from M/s Ashirwad Industries (Punjab, India).

Animals. The experiments were performed on pathogen-free young male Wistar rats of 100−120 g after the study was cleared by the Institutes Animal Ethics Committee. The animals were obtained from the Central Animal House of Postgraduate Institute of Medical Education and Research (Chandigarh). Animals were allowed free access to water and normal pellet diet. They were housed in polypropylene cages bedded with sterilized rice husk. Before the experiments were conducted, the animals were acclimatized for 2−3 weeks for the above conditions.

Methods. Preparation of ST Extract. An aqueous extract of smokeless tobacco (AEST) was prepared as described earlier (*19*). The dried yield of AEST was found to be around 1 mg/10 mg (10% dry wt) of "gutkha". AEST was administered orally at low doses of 96 mg/kg body wt/day (L-AEST) for 2 ($L\text{-}AEST_2$) and 28 weeks ($L\text{-}AEST_{28}$) and a high dose of 960 mg/kg body wt/day (H-AEST) for 2 weeks ($H\text{-}AEST_2$) of the lyophilized extract, which was reconstituted in 300 μL of distilled water and orally administered through gavage to the rats.

ST Administration. The required amount of AEST was administered to the animals twice a day. The animals were divided into five groups, each having seven animals. Control groups of animals received 300 μL of distilled water for 2 and 28 weeks, whereas three groups of treated animals received $L\text{-}AEST_2$ and $H\text{-}AEST_2$ for 2 weeks and $L\text{-}AEST_{28}$ for 28 weeks. H-AEST could not be given up to 28 weeks because of toxicity, which led to a drastic reduction in body weight and food intake. The weight of each animal was recorded weekly. The average diet and water consumption were recorded daily. After the required time periods of AEST administration, animals were sacrificed under pentobarbital anesthesia (40 mg/kg body wt, ip injection). Liver, lung, and kidney were excised and perfused with ice-cold perfusion solution (0.15 M KCl and 2 mM EDTA, pH 7.4). Tissues were homogenized in Tris-HCl buffer (50 mM, pH 7.4) in the ratio of 1:3 w/v, and the homogenates were centrifuged at 10000*g* at 4 °C for 30 min to obtain postmitochondrial supernatant (PMS). The PMS was used for the estimation of antioxidant enzyme activities.

Immunohistochemistry. The tissue sections were kept in the oven for 5 min at 80 °C and deparaffinized in xylene (to remove the wax from the sections), rehydrated through graded alcohol (100, 70, 50, and 30%), and finally brought to water (*20*). The tissue sections were incubated for 30 min at room temperature in endogenous block solution (3% H_2O_2:methanol, 1:9 v/v) to quench the endogenous peroxidase activity. Antigen unmasking was carried out by incubating the sections in 10 mM citrate buffer (pH 6.0) for 20 min in a microwave oven. Slides were allowed to cool at room temperature and were washed twice in 0.1% PBS-Triton solution and finally in PBS alone for 5 min. The sections were then incubated with diluted rat−antirabbit primary antibodies (1:100 for CYP1A1, 1A2, and 2E1 and 1:10 for GST-μ) (Chemicon International, United States) at room temperature for 2 h or overnight depending upon the results. After two similar washings with 0.1% PBS-Triton and one washing with PBS alone, the sections were incubated with respective HRP-labeled antirabbit secondary antibody for 1−2 h at room temperature. Thereafter, sections were washed three times in PBS, and chromogen DAB was added for 2−5 min for color development. After they were washed with distilled water, the sections were counterstained with hematoxylin. Finally, sections were subjected to alcohol and xylene baths, air-dried, and then mounted for examination under a light microscope. Protein expression was evaluated by intensity grading of the color expressed, and the sections were compared with the respective controls. Expression of the enzymes was graded arbitrarily as weak, grade I; moderate, grade II; and strong, grade III.

Micronuclei Assay. A micronuclei assay was performed as described earlier (*21*). Briefly, slides were coated with 0.1% AO in distilled water by keeping them dipped in an AO-filled coupling jar overnight and drip dried in air at room temperature. A drop of blood from the tail vein of mice was collected at regular intervals from week 1 to week 40 after L-AEST administration and was dripped on the slide and covered with a glass slip. Slides were kept in a humid chamber for 4 h at ambient temperature or left overnight in a refrigerator prior to scanning. Slides were coded and scanned

for micronucleated blood reticulocytes under oil immersion (100×) using a fluorescent microscope (BX-51 Olympus, United States).

DNA Fragmentation. After AEST treatment, one of the earliest changes denoting cell death is the activation of a calcium-dependent endonuclease and associated DNA fragmentation (*22*). DNA was extracted as follows: 0.1 mg of tissue was homogenized with 1 mL of lysis buffer containing 100 mM Tris-HCl, pH 7.5, 10 mM EDTA, 10 mM NaCl, 0.4 mg/mL proteinase K (Roche Diagnostics GmbH, Mannheim, Germany), and 0.5% SDS. The solution was incubated at 50 °C for 3 h. DNA was extracted by phenol/chloroform/3-methylbutan-1-ol (25:24:1, v/v/v) solution, precipitated with 95% (v/v) ethanol, washed, dried, and dissolved in 200 μL of TE buffer [10 mM Tris/HCl (pH 7.5)/1 mM EDTA]. Then, it was treated with 0.2 mg/mL DNase-free RNase (Roche) at 37 °C for 2 h and quantified spectrophotometrically at 260 nm. After electrophoresis on 2% (w/v) agarose gel, the DNA fragments in the gel were revealed by staining with ethidium bromide (Molecular Imager Gel Doc System, Biorad Laboratories, United States).

Tumor Necrosis Factor-α (TNF-α) Production. Rat TNF-α was estimated using a solid phase sandwich enzyme-linked immunosorbent assay (ELISA) method in a 96-well plate as per the instructions provided by the kit manufacturer (Diaclone Pvt. Ltd., Besancon Cedex, France). A polyclonal antibody specific for rat TNF-α is coated onto the wells of the microtiter strips. Briefly, to 100 μL of plasma, 50 μL of biotinylated antibody was added in each well. The mixture was incubated for 3 h at room temperature. The samples were washed three times to remove unbound antigen/antibody. Later, 100 μL of streptavadin−HRP was added and incubated for 30 min at room temperature and washed three times to remove excess and unbound enzymes, and then, 100 μL of TMB (a coloring agent) was added. The plate was incubated for 15 min at room temperature in a dark place. The reaction was stopped by adding 100 μL of H_2SO_4, and the absorbance was read at 450 nm in an ELISA plate reader (Merck MIOS Junior, United States).

Myeloperoxidase (MPO) Activity. The MPO activity was measured according to the earlier method (*23*). In brief, the tissue samples were homogenized in 50 mmol/L potassium phosphate buffer (pH 6.0). The homogenate was centrifuged at 10000*g* for 15 min at 4 °C. The supernatant was discarded, and the pellet was resuspended in HTAB (0.5% w/v in 50 mmol/L potassium phosphate buffer, pH 6.0). The suspensions were sonicated on ice and centrifuged at 12000*g* for 15 min at 4 °C. The supernatants were diluted in potassium phosphate buffer (pH 6.0) containing 0.167 mg/mL *o*-dianisidine dihydrochloride and 0.005% H_2O_2. Changes in the absorbance at 450 nm, every 10 s over 2 min, were recorded with a spectrophotometer (Spectronix, United States). One unit of MPO activity was defined as the quantity of MPO degrading 1 μmol H_2O_2/mg protein/min at 25 °C by using the extinction coefficient of $11 \times 103\ M^{-1}\ cm^{-1}$.

Caspase-3 Activity. Caspase-3 activity was performed according the method of Thornberry (*24*). In brief, tissue PMS samples (50−150 μL) were added to the 96-well microplate containing 32 μL of caspase assay buffer (312 mM HEPES, pH 7.5, 31.25% w/v sucrose, and 0.3125% w/v CHAPS), 8 μL of DMSO, 10 μL of 100 mM dithiothreitol, and 5 μL of 10 mM Ac-DEVD-pNA substrate, and the final volume was made up to 200 μL using deionized water. The reaction mixture was incubated for 4 h at 37 °C. The standard curve was plotted taking *para*-nitroaniline (pNA) as a standard. Cleavage of the dye (pNA) from the substrate by the sample increased its yellow intensity, and the maximum absorption was measured using microplate reader at 405 nm (Merck MIOS Junior).

Carbonyl Estimation. Carbonyl estimation was performed following the manufacturer's instructions (Cayman Chemicals Co., MI). Approximately 300 mg of tissue from lung, liver, and kidney was homogenized in 1−2 mL of buffer (50 mM phosphate, pH 6.7, and 1 mM EDTA), and the supernatant was obtained by centrifugation at 10000*g* for 15 min at 4 °C. The carbonyl assay required 300 μL of homogenized tissue sample, which was mixed with 33.3 μL of streptomycin followed by centrifugation at 5000*g* for 10 min. Then, 840 μL of 2.5 M HCl and 840 μL of 20 mM DNPH were added. The tubes were vortexed for a period of 1 h followed by the addition of 840 μL of 20% TCA. Tubes were placed in an ice bath for 10 min and centrifuged for 10 min at 5000*g*. After centrifugation, the pellets were washed out four times with 840 μL of ethanol. The protein samples were resuspended in 840 μL of guanidine hydrochloride. These solutions were centrifuged and incubated at 37 °C in a water bath for 10 min. Finally, the carbonyl contents were analyzed by measuring the absorbance at 370 nm and using an extinction coefficient value of $22 \times 103\ M^{-1}\ cm^{-1}$. Spectrophotometric assays were done with a spectrophotometer (Spectronic Genesys2, United States) supplied by Rochester (NY).

Gene Expression: RNA Isolation and Quantification. The total RNA was extracted from lung, liver, and kidney of rat using an acid guanidinium thiocyanate/phenol/chloroform extraction method (*25*). Briefly, tissues (100 mg) were homogenized in 1 mL of solution I (4 M guanidinium isothiocyanate, 0.5% mercaptoethanol, and 0.3 M sodium acetate, pH 4.0). The homogenate was then extracted with 1 mL of solution II [chloroform/2-methyl-1-propanol (2:1; v/v)] by vigorous mixing, followed by centrifugation for 1 min at 2000*g*. The top aqueous layer was removed, the interface was reextracted with another 200 μL of solution I, and the phases were separated by centrifugation at 12000*g* for 5 min. Then, 1 mL of aqueous extract was diluted with 1 mL of solution III (1% sodium *N*-lauroylsarcosinate), and 2 mL of solution IV [chloroform/acidified phenol (1:4; v/v)] was added, vortexed vigorously, and centrifuged for 10 min at 12000*g*. The top aqueous phase was removed, and 2−3 vol of chilled ethanol (100%, −20 °C) was added, mixed, and centrifuged at 12000*g* for 20 min at 4 °C. The pellet was then washed with 70% ethanol, dried, and analyzed. Approximately 5 μL of the isolated RNA was dissolved in 995 μL of distilled water, and the optical density of the sample was measured at 260 and 280 nm using UV spectrophotometer for quantitative and qualitative measurement of RNA.

Calculation. The concentration of RNA was calculated using the following formula:

$$\text{concentration of RNA } (\mu g/mL) = OD_{260} \times 40\ \mu g/mL \times \text{dilution factor}$$

cDNA Preparation. cDNA preparation was performed following the manufacturer's instructions (Invitrogen Technologies, United States). cDNA was generated from 2 μg of RNA by reverse transcriptase with random hexamers as primers (Table 1). To ensure that the RNA is not degraded, a PCR assay for 40 cycles (94 °C, 1 min; 55 °C, 1 min; and 72 °C, 1 min) and a final extension at 72 °C for 7 min with primers specific for β-actin were carried out on each cDNA sample. Equal amounts of RNA (2 μg) were used in the RT reaction, using oligo $(dT)_{23}$ as the primer, to generate the first-strand cDNA and SuperScriptTM reverse transcriptase (200 units/μL) (Invitrogen Life Technologies, Frederick, MD), following the instructions of the manufacturer. The cDNA was used as a template for amplification in PCR, and we used 2 μL of the first-strand reaction for PCR. The conditions for each PCR were determined in preliminary experiments and optimized for each set of primers. Expression levels of various genes were determined using the following specific primers (5′−3′), and conditions are shown in Table 1:

Agarose Gel Electrophoresis. Agarose gel was prepared according to the earlier described method (*26*). The resulting PCR products were separated by electrophoresis in a 1.5% (w/v) agarose gel in 0.5× TBE (45 mM Tris/45 mM boric acid/1 mM EDTA, pH 8.0) at 5−10 v/cm. The loading gel dye 6× (0.25% bromophenol blue, 0.25% xylene cyanol, and 30% glycerol) was used for loading the samples. Ethidium bromide (0.5 μg) was used for staining the agarose gel. The gel was then visualized on a UV transilluminator (UVP Inc., United States) and photographed. A 100 bp DNA ladder (MBI Fermentas, Germany) was also run in parallel to the PCR product. The expected sizes for the PCR products were as follows: Bcl-2, 501 bp; Bax, 146 bp; p53, 588 bp; NF-kB, 493 bp; and β-actin, 566 bp.

Table 1. Primer Sequence Used for Reverse Transcriptase PCR Reactions

genes	primer sequence (5′ to 3′)	PCR conditions		product size
		temperature	cycle no./min	
Bcl-2	F′-TATGATAACCGGGAGATCGTG	denaturation, 95 °C	1 cycle/5 min	501bp
	R′- CAGATGCCGGTTCAGGTACTC	annealing, 52 °C	37 cycles/1 min	
		amplification, 72 °C	37 cycles/1 min	
Bax	F′- TGGTTGCCCTTTTCTACTTTG	denaturation, 95 °C	1 cycle/5 min	146bp
	R′-GAAGTAGGAAAGGAGGCCATC	annealing, 62 °C	35 cycles/1 min	
		amplification, 72 °C	35 cycles/1 min	
P53	F′-CACAGTCGGATATGAGCATC	denaturation, 95 °C	1 cycle/5 min	588bp
	R′-GTCGTCCAGATACTCAGCAT	annealing, 58 °C	35 cycles/1 min	
		amplification, 72 °C	35 cycles/1 min	
NF-κB	F′-AAGATCAATGGCTACACGGG	denaturation, 95 °C	1 cycle/5 min	493bp
	R′- CCTCAATGTCTTCTTTCTGC	annealing, 64 °C	35 cycles/1 min	
		amplification, 72 °C	35 cycles/1 min	
β-actin	F′-CACTGTGCCCATCTATGAGGG	denaturation, 95 °C	1 cycle/5 min	566bp
	R′-TCCACATCTGCTGGAAGGTGG	annealing, 56 °C	40 cycles/1 min	
		amplification, 72 °C	40 cycles/1 min	

Table 2. Phase I and Phase II Drug-Metabolizing Enzyme Primer Sequences Used for RT-PCR Reactions

target gene	primer sequence (5′−3′)	
	forward	reverse
CYP1A1	CCAAACGAGTTCCGGCCT	TGCCCAAACCAAAGAGAATGA
CYP1A2	CGCCCAGAGCGGTTTCTTA	TCCCAAGCCGAAGAGCATC
CYP2E1	AAAGCGTGTGTGTGTTGGAGAA	AGAGACTTCAGGTTAAAATGCTGCA
GST-μ	GGCGACGCTCCCGACTATGACAGAA	AATCCGCTCCTCCTCTGTCTCTCCA
GAPDH	ATGACTCTACCCACGGCAAG	CTGGAAGATGGTGATGGGTT

Real-Time PCR (RT-PCR). For examining the organ distribution of various xenobiotic drug-metabolizing enzyme expressions after AEST exposure, total RNA was isolated and reverse transcribed, the resulting cDNA was diluted, and quantitative PCR was performed for CYP1A1, CYP1A2, CYP2E1, GST-μ, and the housekeeping gene, GAPDH. The forward and reverse primers used in the present study are listed in Table 2. The quantitative RT-PCR was performed using the ABI Prism 7500 System (Applied Biosystems). The reaction was carried out in a 25 μL final reaction volume containing 10 μM forward and reverse primers (each with a final concentration of 40 nM), 2 μL of cDNA, 10 μL of H_2O, and 12 μL of SYBR Green Universal Mastermix (Applied Biosystems). The thermal profile for the RT-PCR was 95 °C for 10 min, followed by 40 cycles of denaturation at 95 °C for 1 min, annealing at 60 °C for 1 min (40 cycles), and extension at 72 °C for 1 min (40 cycles), followed by a final extension at 72 °C for 7 min. The specificity of the primers and the purity of the final PCR products were assessed by performing the melting curves by the end of each cycle. The relative quantification of the expression of the target genes was measured using GAPDH (glyceraldehydes-3-phosphate dehydrogenase) mRNA as an internal control according the instructions in Applied Biosystems bulletin. The data are presented as a fold change in gene expression normalized to endogenous reference gene GAPDH using an untreated control as a calibrator.

Statistics. Values were expressed as mean ± SEM. Statistical analysis was performed by the unpaired Student's *t* test; $p < 0.05$ was considered as significant.

Results

Body Weight, Diet Intake, and Water Consumption. Oral administration of L-$AEST_2$, L-$AEST_{28}$, and H-$AEST_2$ to the animals had no significant change in the body weight, diet, and water intake as compared to their respective control animals (Figure 1).

Xenobiotic Drug-Metabolizing Enzymes Expression. CYP1A1. Immunohistological expression of CYP1A1 in various tissues is shown in Figure 2. Administration of H-$AEST_2$ and L-$AEST_{28}$ enhanced the expression of CYP1A1 to grade II and grade III levels, respectively, with increased infiltration of alveolar macrophages in the interstitial epithelium of the lung

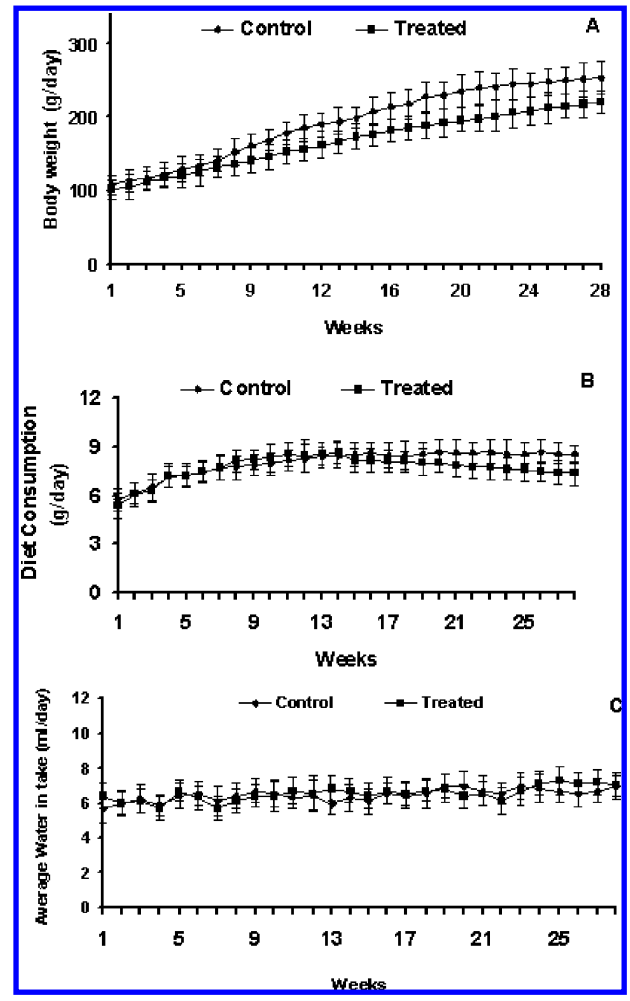

Figure 1. Effect of oral administration of a low dose of AEST (L-AEST) (96 mg/kg body wt/day) for 28 weeks on the body weight (A), diet consumption (B), and water intake (C) of male rats. Values are means ± SEMs, $n = 7$. No significant change was observed in the body weight, diet, and water intake in AEST-treated rats as compared to their respective controls.

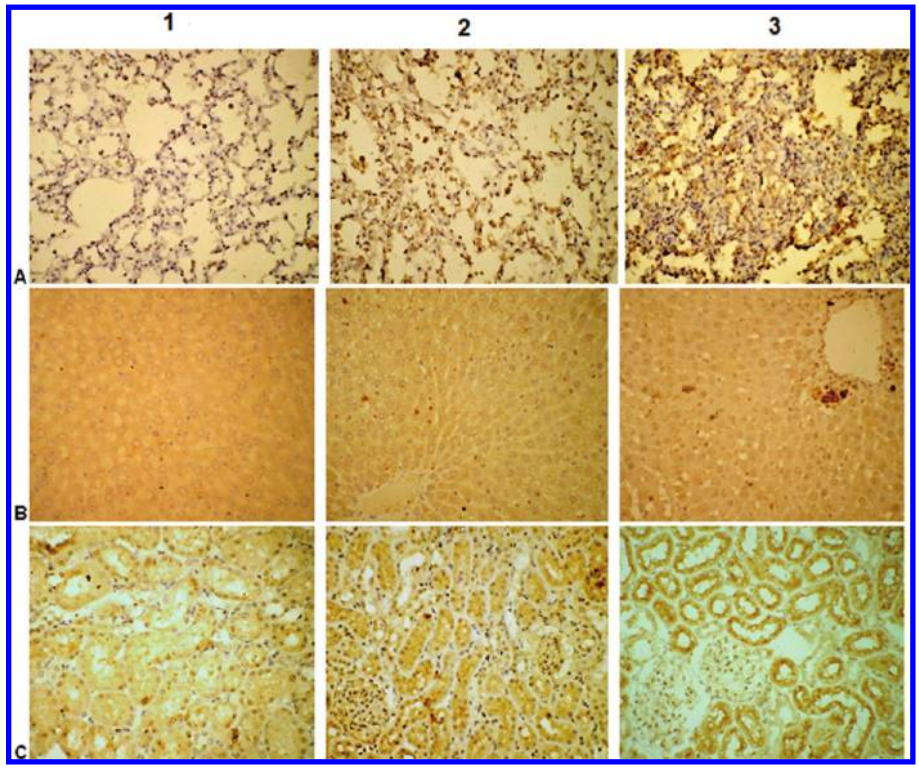

Figure 2. Immunohistochemical expression of CYP1A1 in lung (A), liver (B) and kidney (C) of rats (Column 1; normal), after oral administration of high dose of AEST for 2 weeks (H-AEST$_2$ - 960 mg/kg body wt/day) (Column 2) and low dose for 28 weeks (L-AEST$_{28}$ - 96 mg/kg body wt/day) (Column 3) (Peroxidase-antiperoxidase, X400). The figures indicate A, (1) Normal lung morphology - no expression for CYP1A1; (2) grade-I cytoplasmic positivity in alveolar type-I epithelial cells and macrophages; (3) grade-III cytoplasmic positivity in alveolar type-I epithelial cells. B, (1) Normal liver - no expression for CYP1A1; (2) grade-I diffused cytoplasmic expression in hepatocytes around the centrilobular region; (3) grade-III cytoplasmic granular expression in hepatocytes around the centrilobular region. C, (1) Normal kidney with mild grade-I cytoplasmic expression in proximal tubules; (2) grade-II cytoplasmic expression in the proximal tubules; (3) grade-III cytoplasmic expression in the proximal tubules.

(Figure 2A, 2 and 3). Quantitative PCR showed 3.98- and 9.13-fold increases in CYP1A1 gene expression in lung at the above doses (Figure S4A in the Supporting Information). In the case of liver, H-AEST$_2$ and L-AEST$_{28}$ caused diffused induction of cytoplasmic protein expression of CYP1A1 to grade I and grade III, respectively, in the hepatocytes around the centrilobular region in a diffused manner (Figure 2B, 2 and 3). Liver CYP1A1 gene expression was significantly increased to 2.73- and 4.86-fold in H-AEST$_2$- and L-AEST$_{28}$-treated rats. In the case of kidney, H-AEST$_2$ and L-AEST$_{28}$ increased cytoplasmic protein expression of CYP1A1 to grade II and grade III, respectively, in the proximal tubules (Figure 2C, 2 and 3). CYP1A1 gene expression was significantly expressed to 3.18- and 6.76-fold in kidney on treatment with H-AEST$_2$ and L-AEST$_{28}$ as compared to the control (Figure S4A in the Supporting Information).

CYP1A2. Immunohistological and gene expression of CYP1A2 in various tissues are shown in (Figure S1 in the Supporting Information). There was grade I cytoplasmic positivity of CYP1A2 expression in the alveolar type I epithelial cells in the normal control lung. H-AEST$_2$ showed grade II cytoplasmic expression of CYP1A2 in the alveolar type II epithelial cells, whereas L-AEST$_2$ showed grade III CYP1A2 expression in alveolar type I and type II epithelial cells. In the case of liver, administration of H-AEST$_2$ enhanced the expression of CYP1A2 only in the Kupffer cells, which infiltrated in the hepatocytes. However, L-AEST$_{28}$ induced grade II CYP1A2 expression not only in the Kupffer cells but also in the hepatocytes. In the case of kidney, H-AEST$_2$ and L-AEST$_{28}$ induced grade II and grade III cytoplasmic expression of CYP1A2 in the distal tubules. The gene expression profiles in rat lung, liver, and kidney after treatment with H-AEST$_2$ and L-AEST$_{28}$ were significantly enhanced as shown in Figure S4B in the Supporting Information. Liver showed the highest expression of CYP1A2 gene after treatment with H-AEST$_2$ (3.96-fold) and L-AEST$_{28}$ (6.67-fold) as compared to lung (3.23- and 4.86-fold) and kidney (2.88- and 4.92-fold), respectively.

CYP 2E1. Protein and gene expression of CYP2E1 in various tissues are shown in Figures S2 and S4C in the Supporting Information. There was a mild cytoplasmic positivity of CYP2E1 in alveolar type I epithelial cells of normal lung tissue, which was enhanced to grade II and grade III on administration of H-AEST$_2$ and L-AEST$_{28}$, respectively, in both alveolar type I and type II epithelial cells. The transcriptional level expression of CYP2E1 increased to 3.76- and 5.11-fold after administration of H-AEST$_2$ and L-AEST$_{28}$, respectively (Figure S4C in the Supporting Information). In the liver, H-AEST$_2$ and L-AEST$_{28}$ administration caused grade I and grade III cytoplasmic expression of CYP2E1, respectively, in the hepatocytes around the centrilobular region. CYP2E1 gene expression in liver increased to 5.57- and 10.14-fold after H-AEST$_2$ and L-AEST$_{28}$ administration as compared to their respective controls (Figure S4C in the Supporting Information). In normal kidney, there was grade I expression in the epithelial cells lining the proximal tubules, which was enhanced to grade II after administration of H-AEST$_2$ and L-AEST$_{28}$. Although CYP2E1 gene expression was significantly enhanced in kidney, it was the least expressed as compared to lung and liver at both of the doses (Figure S4C in the Supporting Information).

GST-μ. Immunohistological expression of GST-μ in various tissues is shown in Figure S3 in the Supporting Information. In normal lung, there was grade I GST-μ expression in the alveolar

type I epithelial cells, which did not change after treatment with L-AEST$_2$. However, administration of H-AEST$_2$ and L-AEST$_{28}$ enhanced its expression to grade II and grade III levels, respectively, in both type I and II epithelial cells. Interestingly, in liver, there was no significant change in the expression of GST-μ at all of the doses administrated to the animals. In the case of kidney, H-AEST$_2$ and L-AEST$_{28}$ produced grade II and grade III granular cytoplasmic expression in proximal tubules, respectively. Quantitative gene expression studies of GST-μ after treatment with H-AEST$_2$ and L-AEST$_{28}$ showed significant enhancement in all of the organs (Figure S4D in the Supporting Information). The expression of GST-μ gene in lung and kidney was higher than the liver at both of the AEST doses.

Chromosomal Damage Assessment by Micronuclei Formation. The micronucleus assay is a method to assess the chromosomal aberrations caused due to the genotoxic or clastogenic effects of AEST. Chromosomal damage and breakage in peripheral blood mononuclear cells result in DNA fragments, which form micronuclei that remain in the mature cell. This can be detected by the use of fluorescent dye AO and is easily scored by fluorescence microscopy (Figure 3A). Normal chromosomes as indicated by the intense green fluorescence (Figure 3A, 1−4), initiation of AEST-induced damage as indicated by yellow fluorescence (Figure 3A, 5), and intense damage to the genomic material as indicated by red fluorescence (Figure 3A, 6), respectively. Oral administration of L-AEST$_2$ or H-AEST$_2$ did not show any significant change in the micronuclei formation in peripheral blood mononuclear cells in rats as compared to the control. However, L-AEST$_{28}$ treatment led to the increased formation of micronuclei as shown by arrows (Figure 3A), which increased by 7-fold (from 2 to 14%) (Figure 3B).

Plasma TNF-α Levels. Treatment of rats with L-AEST$_2$ and H-AEST$_2$ changed the plasma TNF-α level from 50.82 ± 10.71 (control) to 61.94 ± 15.61 and 62.48 ± 14.73 pg/mL, respectively, which was not significant. However, administration of L-AEST$_{28}$ significantly increased ($p < 0.05$) the TNF-α level by more than 100% to 127.67 ± 13.67 pg/mL (Table 3).

MPO Activity in the Tissues. Changes in the MPO activity in the lung, liver, and kidney were assessed after the administration of AEST for different time periods to rats (Table 3). L-AEST$_{28}$ significantly increased lung MPO activity by 108% from 4.4 ± 1.10 to 9.17 ± 2.47 μmol H_2O_2/mg protein/min. No significant change was found in the MPO activity of the liver in the control and L-AEST$_2$- and H-AEST$_2$-treated rats, whereas it increased by 88% from 3.49 ± 1.23 (control) to 6.57 ± 1.41 μmol H_2O_2/mg protein/min in the L-AEST$_{28}$-treated group. Similarly, the administration of L-AEST$_{28}$ significantly increased the MPO activity in the kidney by 151%, that is, from 3.23 ± 1.09 to 8.12 ± 2.37 μmol H_2O_2/mg protein/min ($p < 0.05$).

Protein Carbonyl Formation. AEST-induced oxidation of proteins leads to the formation of protein carbonyls, a marker for the oxidative stress of the cellular protein damage. Table 3 shows the changes in the protein carbonyl content in lung, liver, and kidney after the administration of L-AEST$_2$, L-AEST$_{28}$, and H-AEST$_2$. The protein carbonyl contents in the control lung, liver, and kidney were 1.32 ± 0.62, 1.26 ± 0.73, and 1.24 ± 0.67 ng/mg protein, which did not change significantly after oral administration of L-AEST$_2$ and H-AEST$_2$. However, L-AEST$_{28}$ significantly ($p < 0.05$) enhanced the protein carbonyl content in the lung, liver, and kidney by 235, 166, and 196%, respectively, as compared to their respective controls.

Caspase-3 Activity in Tissues. Changes in caspase-3 activity, a marker for the irreversible activation of apoptotic pathways, in the lung, liver, and kidney of rats were assessed after the administration of AEST. Caspase-3 activities in the control lung, liver, and kidney were found to be 6.60 ± 1.95, 7.94 ± 1.88, and 3.5 ± 1.14 nmol pNA/mg protein/h, respectively (Table 3). However, administration of L-AEST$_2$ or H-AEST$_2$ did not significantly alter the enzyme activities in these organs, whereas L-AEST$_{28}$ significantly increased ($p < 0.05$) the caspase-3 activity by 302, 955, and 222% in the lung, liver, and kidney, respectively, as compared to their respective controls.

DNA Fragmentation. Figure 4 shows the DNA fragmentation in lung, liver, and kidney induced by the administration of AEST. L-AEST$_2$ and H-AEST$_2$ did not induce the DNA fragmentation in lung, liver, and kidney of rats as observed in lanes 3 and 4 of Figure 4A−C. However, L-AEST$_{28}$ caused DNA fragmentation in these organs (lane 5, Figure 4A−C). The DNA fragmentation pattern was more pronounced in the liver followed by lung and kidney.

Gene Expression. For all of the genes, densitometric analysis of PCR products is shown in Figure 5.

P53. AEST-induced changes in the p53 gene expression in lung, liver, and kidney are shown in Figure 5. There was no significant change in the P53 gene expression in lung, liver, and kidney after L-AEST$_2$ administration (lane 3, Figure 5A), whereas H-AEST$_2$ significantly enhanced the p53 gene expression in lung and kidney by 110 and 40%, respectively, without any affect in the expression in the liver. On the other hand, L-AEST$_{28}$ induced p53 gene in all of the organs of the rat, that is, lung, liver, and kidney, by 167, 70, and 112%, respectively (Figure 5A).

Bax. No significant change in the Bax (pro-apoptotic) gene expression in lung, liver, and kidney was observed when the animals were orally administered with L-AEST$_2$ or H-AEST$_2$ (lanes 3 and 4 of Figure 5B). However, administration of L-AEST$_{28}$ significantly enhanced the expression of Bax by 189, 190, and 123% in lung, liver, and kidney, respectively, as compared to the control (Figure 5B).

Bcl-2. Bcl-2 expression in lung, liver, and kidney remained unaltered after the oral administration of L-AEST$_2$ (lane 3, Figure 5C), whereas administration of H-AEST$_2$ significantly decreased the expression of Bcl-2 in lung, liver, and kidney by 28, 14, and 26%, respectively. Furthermore, administration of L-AEST$_{28}$ also significantly declined the gene expression by 36, 35, and 37% in lung, liver, and kidney, respectively, as compared to the control.

NF-kB. Oral administration of L-AEST$_2$ did not change the expression levels of NF-kB in lung, liver, and kidney (lane 3, Figure 5D). However, administration of L-AEST for 28 weeks significantly increased the expression of NF-kB in lung, liver, and kidney by 212, 140, and 312%, respectively, whereas administration of H-AEST$_2$ increased its expression only in lung and kidney by 56 and 97%, respectively.

Discussion

Chronic use of ST leads to inflammation in the oral mucosa by the enhanced expression of inflammatory cytokines and expression of CYP450 (*27, 28*). However, the information on the effects of ST on other organs and isozymes of CYP450 is still lacking. Administration of L-AEST$_{28}$ induced the CYP1A1 and 2E1 protein expression in the liver around the centrizonal region and CYP1A2 expression in the Kupffer cells. Although immunohistological studies were performed to evaluate the anatomical changes and expression profile of phase I and phase

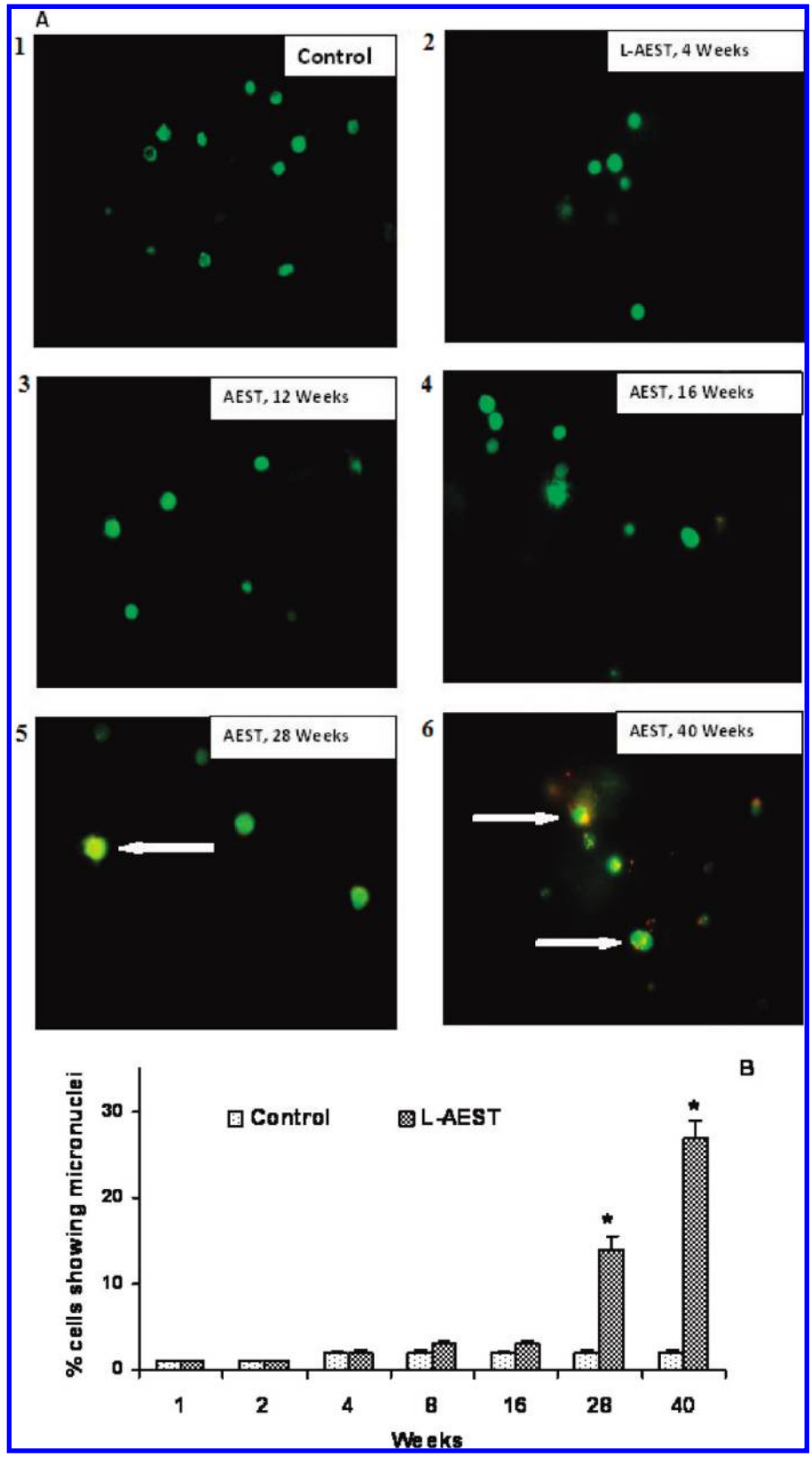

Figure 3. Effect of oral administration of L-AEST (96 mg/kg body wt/day) up to 40 weeks on the formation of micronuclei in the peripheral blood mononuclear cells (PBMCs) of male rats. The fluorescence images were obtained by staining the mononuclear cells with the fluorescent dye, AO, of the control and AEST-treated animals as shown in panel A. The arrows indicate the presence of micronuclei formation in PBMCs. The green color indicates the normal genetic material (images 1−4), the yellow color indicates the initiation of chromosomal damage (image 5), and the most intense red color indicates the extensive chromosomal damage (image 6). The number of micronucleated mononuclear cells/200 cells counted/field view is represented in terms of % cells showing micronuclei (B). Values are means ± SEMs, $n = 7$; $*p < 0.05$ is considered significant as compared to the control.

II enzymes in different organs before and after AEST administration, RT-PCR was performed for quantitative analysis of these isoforms. Although in rodents CYP1A2 is abundantly expressed in liver, poor expression of CYP1A2 in normal liver and intense expression in AEST-treated lung and kidney might be binding of the antibody to a different protein.

Table 3. Effect of AEST on Plasma TNF-α, MPO, Caspase-3 Activity, and Protein Carbonyl Content in Lung, Liver, and Kidney[a]

	treatment with AEST				
	2 weeks			28 weeks	
parameters[b]	control	low dose[c]	high dose[d]	control	low dose[c]
plasmaTNF-α	50.82 ± 10.62	61.943 ± 15.61	62.48 ± 14.73	62.42 ± 12.91	127.67 ± 13.67*
			MPO		
lung	3.12 ± 1.22	3.63 ± 1.06	4.67 ± 1.53	4.4 ± 1.1	9.17 ± 2.47*
liver	2.96 ± 0.93	3.56 ± 1.27	4.19 ± 1.49	3.49 ± 1.23	6.57 ± 1.41*
kidney	3.16 ± 1.23	3.72 ± 1.34	4.12 ± 1.62	3.23 ± 1.09	8.12 ± 2.37*
			protein carbonyl content		
lung	1.32 ± 0.62	1.63 ± 0.61	2.17 ± 0.73	1.4 ± 0.91	4.7 ± 0.67*
liver	1.26 ± 0.73	1.56 ± 0.47	1.77 ± 0.67	1.34 ± 0.72	3.57 ± 0.83*
kidney	1.24 ± 0.67	1.72 ± 0.71	2.12 ± 0.82	1.39 ± 0.79	4.12 ± 0.88*
			caspase-3 activity		
lung	6.6 ± 1.946	6.96 ± 2.44	9.76 ± 2.1	4.4 ± 1.2	17.7 ± 1.56*
liver	7.94 ± 1.88	7.78 ± 1.23	10.19 ± 1.72	5.23 ± 1.78	55.2 ± 3.12*
kidney	3.05 ± 1.14	3.78 ± 2.1	5.09 ± 1.2	3.83 ± 0.76	12.37 ± 1.91*

[a] Values are means ± SEMs; $n = 7$. *$p < 0.05$ as compared to the control. [b] Plasma TNF-α, pg/mL; MPO activity, μmol H_2O_2/min/mg protein; protein carbonyl, ng/mg protein; and caspase-3 activity, nmol pNA liberated/h/mg protein. [c] Low dose (96 mg/kg body wt/day). [d] High dose (960 mg/kg body wt/day).

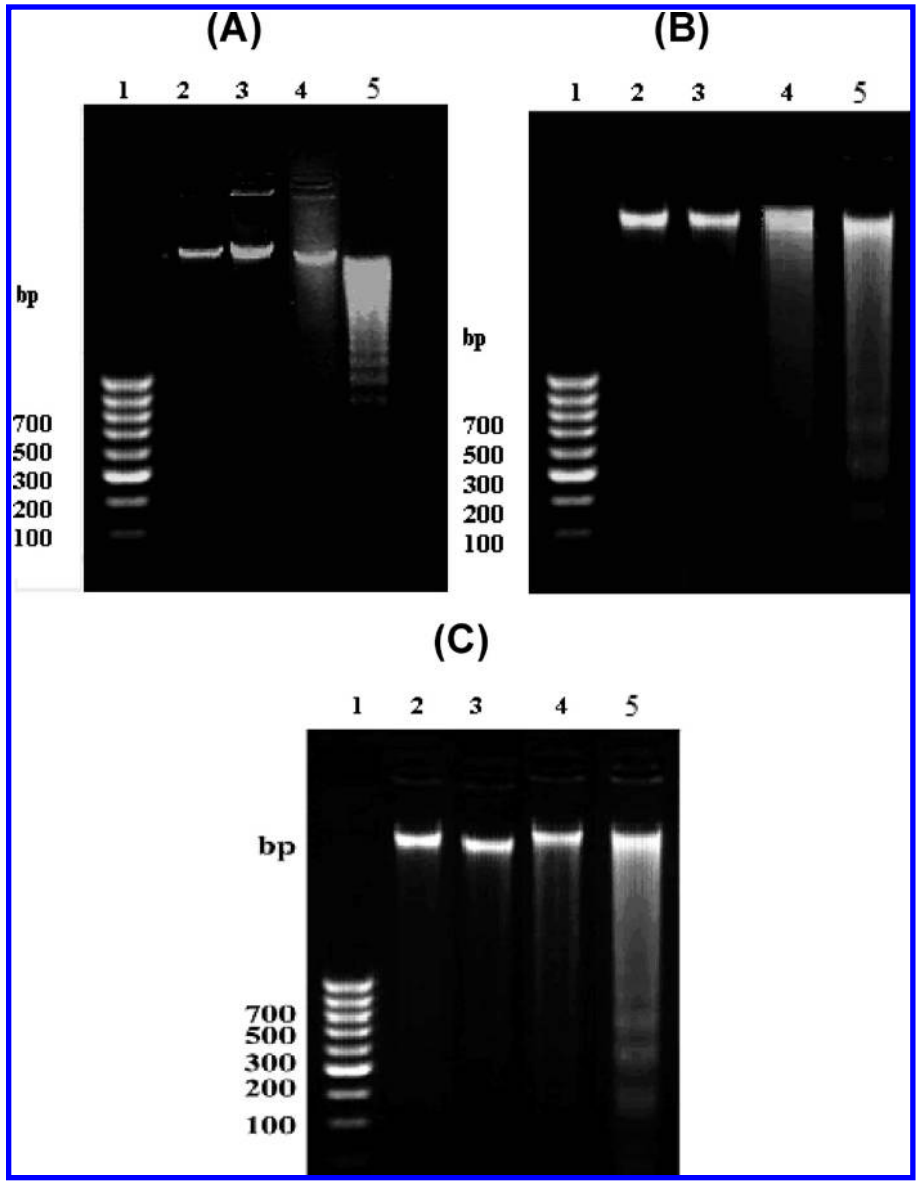

Figure 4. DNA fragmentation in lung (A), liver (B), and kidney (C) of rats after oral administration of AEST at low dose (96 mg/kg body wt/day) for 2 (L-$AEST_2$) and 28 weeks (L-$AEST_{28}$) and at high dose (960 mg/kg body wt/day) for 2 weeks (H-$AEST_2$). Lane 1, marker; lane 2, control; lane 3, L-AEST for 2 weeks; lane 4, H-AEST for 2 weeks; and lane 5, L-AEST for 28 weeks.

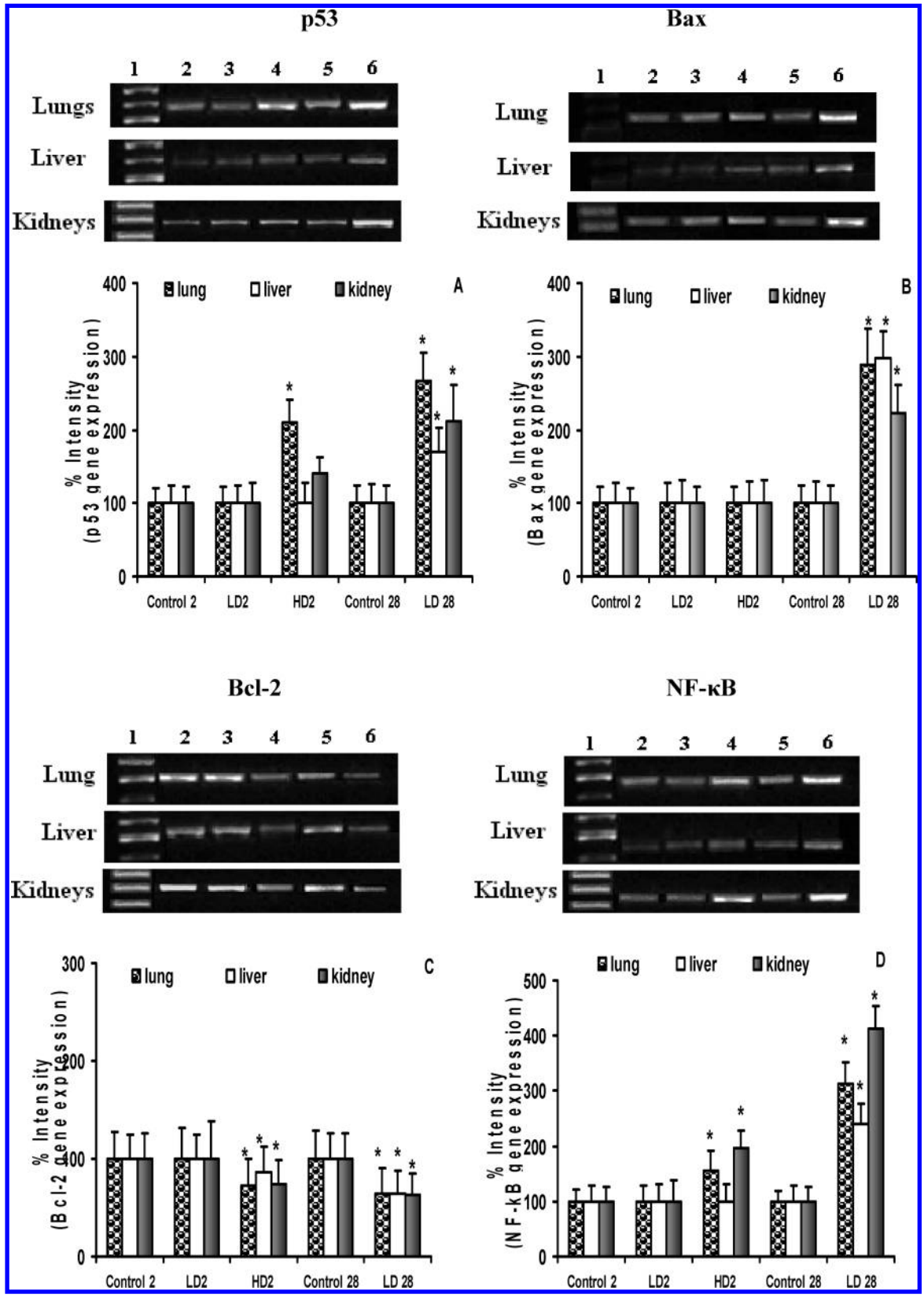

Figure 5. Gene expression of p53 (A), Bax (B), Bcl-2 (C), and NF-κB (D) in lung, liver, and kidney of rats after oral administration of low dose (96 mg/kg body wt/day) for 2 (L-AEST$_2$) and 28 weeks (L-AEST$_{28}$) and H-AEST (960 mg/kg body wt/day) for 2 weeks (H-AEST$_2$). Lane 1, marker; lane 2, control for 2 weeks; lane 3, L-AEST for 2 weeks; lane 4, H-AEST for 2 weeks; lane 5, control for 28 weeks; and lane 6, L-AEST for 28 weeks. Densitometric analysis of the PCR products of p53 (A), Bax (B), Bcl-2 (C), and NF-kB (D) genes after oral administration of AEST in rats. The values for controls from untreated animals were taken as 100%. The data are represented as means ± SDs of five assays. The abbreviations in the figure are as follows: control 2, control for 2 weeks; LD2, low dose of AEST (96 mg/kg body wt/day) for 2 weeks; HD2, high dose of AEST (960 mg/kg body wt/day) for 2 weeks; control 28, control for 28 weeks; and LD28, low dose of AEST (96 mg/kg body wt/day) for 28 weeks. Values are means ± SEMs, $n = 5$; $^*p < 0.05$ significantly different as compared to the control.

As any cytotoxic substance that gets absorbed through the intestinal mucosa into the portal system would be exposed to the centrizonal hepatocytes to the maximum extent, an enhanced expression of CYP1A1 and 2E1 in the centrizonal region was

expected. It was further confirmed at the transcription level by quantitative PCR. This could be due to the AEST compounds competition for differential localization of aryl hydrocarbon receptor (AhR) in the centrilobular versus periportal regions of the liver (*29*) or perhaps through interactions of signal transduction cascades initiated by the different compounds present in AEST (*30*). Expression of CYPs is known to play an important role in Kupffer cells (resident macrophage system in liver) activation in releasing the various mediators such as pro-inflammatory cytokines [TNF-α and interleukins (IL)], including reactive oxygen, nitrogen species, proteases, and lipid metabolites such as prostaglandins and thromboxane (*31, 32*). In the present study, the enhanced level of TNF-α in plasma after administration of L-AEST for 28 weeks also confirms this observation.

Administration of L-AEST for 28 weeks induced intense expression of CYP1A1, 1A2, and 2E1 in type I and type II cells of the lung, whereas in kidney the expression of CYP1A1 and 2E1 was observed in the proximal tubular epithelial cells and CYP1A2 was expressed in the distal tubular epithelial cells, which is due to the presence of a selective set of biotransformation enzymes in these organs (*33, 34*). These results in increased formation of reactive metabolites of carcinogenic material present in ST cause DNA damage if the levels of phase II drug detoxifying enzymes, more specifically GST-μ, get impaired. However, it was in liver GST-μ expression in centrilobular parenchymal cells after L-AEST administration for 28 weeks that was not altered; hence, these cells possess a higher capacity for generating highly reactive and toxic, electrophilic metabolites from endogenous and exogenous substances due to increased levels of CYP enzymes. The abundant and distinct localization of GST-μ in the proximal tubular cells of kidney supports their utilization as a biomarker for determining regioselective renal damage (*35, 36*). Earlier reports suggest that conjugation with reduced glutathione (GSH) resulted in detoxification of the active xenobiotic metabolites (*29, 37, 38*). Under such circumstances, the ability of a cell to detoxify an electrophilic metabolite, as a first line of defense, governs the degree of cytotoxicity. Thus, the relatively low concentrations of GSH in pulmonary, hepatic, and renal tissues as reported by us earlier appear to subsequently lessen the ability of the cells to detoxify these harmful components of AEST, which might ultimately contribute to cytotoxicity (*19*).

As the induction in CYP and GST-μ after administration of L-AEST to the animals was not sufficient to give protection to the body system, further studies related to DNA damage were conducted. AEST-induced chromosomal aberrations in the form of micronuclei were used as cytogenetic end points. Earlier studies report that use of different forms of ST (Maras powder, Gudhaku and Khaini) and smoking induce the formation of micronuclei in the buccal mucosal cells in vitro (*39*−*41*), whereas from our study, it is evident that oral administration of L-AEST produced a toxic/mutagenic effect on the peripheral blood cells as well.

Histological studies revealed that L-AEST mediated moderate infiltration of phagocytic cells such as macrophages, neutrophils, etc. in the portal tract of liver and interstitial spaces of the lung. Administration of L-AEST for 28 weeks induced the MPO activity in lung, liver, and kidney to different extents. MPO, a marker for tissue inflammation and oxidative stress, has been reported to be involved in the metabolism of tobacco components such as polycyclic aromatic hydrocarbons (PAHs) through the action of reactive oxygen species (ROS) such as H_2O_2 (*42*). This MPO-mediated activation may be especially relevant in organs that contain relatively low levels of CYP450. Recent studies report that MPO is implicated in the induction of a variety of DNA base lesions including chlorinated bases (*43, 44*), systemic complex cascade of nonspecific reactions resulting in excessive generation of inflammatory mediators such as cytokines (TNF-α, IL-1, and IL-6), C-reactive protein, and nitric oxide by cells of the innate (macrophages, monocytes, and neutrophils) and adaptive (T-lymphocytes) arms of the immune system. L-AEST-induced tissue inflammation seems to be associated with increased MPO activity and enhanced expression of pro-inflammatory cytokines such as TNF-α.

The induction of p53-mediated oxidative stress is regulated by a redox mechanism, and enhanced expression of glutathione peroxidase (GPx) indicates its direct role in the maintenance of redox homeostasis (*45*). Oxidative stress by AEST was induced due to an imbalance between H_2O_2-producing SOD (superoxide dismutase) and the peroxide-removing enzymes, GPx and CAT (catalase) (*19*). It appears paradoxical that p53, on one hand, induces the genes responsible for ROS generation, which mediates apoptosis (*46*), and, on the other hand, induces expression of a protective antioxidant enzyme, GPx, which protects cells from oxidative damage and apoptosis (*47, 48*). Therefore, the balance between ROS-mediated signaling and activation of redox enzymes determines the ultimate fate of the cells directing toward either apoptosis or survival. p53 expression by L-AEST in the order lung > kidney > liver indicates that the liver might be more susceptible to oxidative stress-mediated damage as compared to other organs because p53-induced GPx might be responsible for stabilizing the effect of oxidative stress in the organs. Another pathway is that L-AEST-induced p53 mediates the cell death directly through the caspase cascade or indirectly through the transcriptional induction of the Bax, a Bcl-2 family gene, in these organs. The Bax gene has a p53-responsive element within its promoter region (*49, 50*), and Bax induction has been observed during p53-mediated cell death in certain cell systems (*51*−*53*). One of the main interesting features of the present study is the observation that L-AEST-induced Bcl-2 family related genes have different expression patterns in different organs. The organs that maintain elevated levels of Bcl-2 are either constantly exposed to an oxygen tension, like in the lung (*54*), or achieve a vast metabolic and energetic activity like the liver. Therefore, an important issue to understand Bcl-2 functions in vivo is to establish its expression in different tissues during stress conditions, which would give us an indication of the susceptibility and sensitivity of these organs toward the AEST-mediated oxidative stress-induced organ damage. Yet, many of these pro-apoptotic members are either constitutively expressed in cells (e.g., Bax) or require an additional step to be active (i.e., Bid requires caspase cleavage to be pro-apoptotic). The reciprocal molecular relationship between Bcl-2 and p53 further highlights the significance of decreased Bcl-2 and enhanced p53 mRNA and caspase-3 levels by AEST. Bcl-2 inhibits p53 transcriptional activity, and the status of Bcl-2 determines apoptotic homeostasis in renal pathologies (*55*). In turn, p53 down-regulates Bcl-2 expression (*56*). Therefore, the direct impact of AEST-induced p53 up-regulation confers limited interpretation as this likely upsets the balance of Bcl-2 family genes rather than reflecting the physiology of each protein and the fate of the cell or tissue. L-AEST-mediated Bcl-2 down-regulation and enhanced Bax expression during oxidative stress conditions in various organs can be inter-

preted as a mechanism causing cell death or cell damage leading to organ damage. A physiological advantage of L-AEST-mediated Bcl-2 down-regulation leading to cell death might be to prevent the DNA-damaged cells from undergoing a repair process and that might enter replicative senescence or accumulation of genetic alterations, contributing to organ deterioration and pathogenesis.

In conclusion, this is the first report that shows differential induction of CYP450 in different organs of Wistar rats by ST. Greater susceptibility of liver toward the damage by ST may be due to deregulation of the activation−detoxification process in this organ as compared to the others. Inflammation in different organs caused by increased levels of plasma TNF-α appears to lead to genotoxic damage. Mechanistic in vivo studies further enhance our understanding in the tobacco-related carcinogenesis and their implications for therapeutic strategy.

Acknowledgment. This work was funded by the Postgraduate Institute of Medical Education and Research (Chandigarh, India).

Supporting Information Available: Immunohistochemical expression of CYP1A2, CYP2E1, and GST-μ and gene expression of CYP1A1, CYP1A2, CYP2E1, and GST-μ. This material is available free of charge via the Internet at http://pubs.acs.org.

References

(1) Bates, C., Fagerström, K., Jarvis, M. J., Kunze, M., McNeill, A., and Ramström, L. (2003) European Union policy on smokeless tobacco: A statement in favor of evidence based regulation for public health. *Tob. Control 12*, 360–367.

(2) Changrani, J., and Gany, F. (2005) Paan and Gutkha in the United States: An emerging threat. *J. Immigrant Health 7*, 103–108.

(3) Indian Council for Medical Research (ICMR) (2001) *Report of the Expert Committee on the Economics of Tobacco Use*, Department of Health, Ministry of Health and Family Welfare, Government of India, New Delhi.

(4) Mukherjee, K., and Hadaye, R. S. (2006) Gutkha consumption and its determinants among secondary school male students. *Ind. J. Community Med. 31*, 177.

(5) Estabrook, R. W. (1996) The remarkable P450s: A historical overview of these versatile hemeprotein catalysts. *FASEB J. 10*, 202–204.

(6) Kessova, I., and Cederbaum, A. I. (2003) CYP2E1: Biochemistry, toxicology, regulation and function in ethanol-induced liver injury. *Curr Mol. Med. 3*, 509–518.

(7) Wattenberg, L. W., and Leong, J. L. (1971) Tissue distribution studies of polycyclic hydrocarbon hydroxylase activity. In *Handbook of Experimental Pharmacology* (Brodie, B. B., and Gillette, J., Eds.) Vol. 28/2, pp 422−430, Springer, Berlin.

(8) Lohr, J. W., Willsky, G. R., and Acara, M. A. (1998) Renal drug metabolism. *Pharmacol. Rev. 50*, 107–141.

(9) Cohen, G. M. (1990) Pulmonary metabolism of foreign compounds: Its role in metabolic activation. *Environ. Health Perspect. 85*, 31–41.

(10) Brown, E. A. B. (1974) The localization, metabolism and effects of drugs and toxicants in lung. *Drug Metab. Rev. 3*, 33–87.

(11) Bend, J. R., Serabjit-Singh, C. J., and Philpot, R. M. (1985) The pulmonary uptake, accumulation and metabolism of xenobiotics. *Annu. Rev. Pharmacol. Toxicol. 25*, 97–125.

(12) Merchant, A., Husain, S. S., Hosain, M., Fikree, F. F., Pitiphat, W., Siddiqui, A. R., Hayder, S. J., Haider, S. M., Ikram, M., Chuang, S. K., and Saeed, S. A. (2000) Paan without tobacco: An independent risk factor for oral cancer. *Int. J. Cancer 86*, 128–131.

(13) Boucher, B. J. (2001) Paan without tobacco: an independent risk factor for oral cancer. *Int. J. Cancer 91*, 592–593.

(14) Stepanov, I., Hecht, S. S., Ramakrishnan, S., and Gupta, P. C. 2005(a) Tobacco-specific nitrosamines in smokeless tobacco products marketed in India. *Int. J. Cancer 116*, 16–19.

(15) Critchley, J. A., and Unal, B. (2003) Health effects associated with smokeless tobacco: A systematic review. *Thorax 58*, 435–443.

(16) Teo, K. K., Ounpuu, S., Hawken, S., Pandey, M. R., Valentin, V., Hunt, D., Diaz, R., Rashed, W., Freeman, R., Jiang, L., Zhang, X., and Yusuf, S. (2006) INTERHEART Study Investigators. Tobacco use and risk of myocardial infarction in 52 countries in the INTERHEART study: A case-control study. *Lancet 368*, 647–658.

(17) Subramanian, S. V., Nandy, S., Kelly, M., Gordon, D., and Smith, G. D. (2004) Patterns and distribution of tobacco consumption in India: Cross sectional multilevel evidence from the 1998−1999 national family health survey. *Br. Med. J. 328*, 801–806.

(18) Jorenby, D. E., Fiore, M. C., Smith, S. S., and Baker, T. B. (1998) Treating cigarette smoking with smokeless tobacco: A flawed recommendation. *Am. J. Med. 104*, 499–500.

(19) Avti, P. K., Kumar, S., Pathak, C. M., Vaiphei, K., and Khanduja, K. L. (2006) Smokeless tobacco impairs the antioxidant defense in liver, lung and kidney of rats. *Toxicol. Sci. 89*, 547–553.

(20) Van Der Loos, C. M. (2000) Immunoenzyme multiple staining methods. In *Microscopy Handbook* (Bosher, A., Ed.) BIOS Scientific Publisher.

(21) Hayashi, M., Morita, T., Kodama, Y., Sofuni, T., and Ishidate, M., Jr. (1990) The micronucleus assay with mouse peripheral blood reticulocytes using acridine orange-coated slides. *Mutat. Res. 245*, 245–249.

(22) Gullicksen, P. S., Dean, R. G., and Baile, C. A. (2004) Detection of DNA fragmentation and apoptotic proteins, and quantification of uncoupling protein expression by real-time RT-PCR in adipose tissue. *J. Biochem. Biophys. Methods 58*, 1–13.

(23) Hillegass, L. M., Griswold, D. E., Brickson, B., and Albrightson-Winslow, C. (1990) Assessment of myeloperoxidase activity in whole rat kidney. *J. Pharmacol. Methods 24*, 285–295.

(24) Thornberry, N. A. (1994) Interleukin-1beta converting enzyme. *Methods Enzymol. 244*, 615–631.

(25) Chomczynski, P., and Sacchi, N. (1987) Single-step method of RNA isolation by acid guanidinium thiocyanate-phenol-chloroform extraction. *Anal. Biochem. 162*, 156–159.

(26) Sambrook, J., Pritsch, E. R., and Miniatis, T. (1989) *Molecular Cloning: A Laboratory Manual*, 2nd ed., Cold Spring Harbour Laboratory Press, Cold Spring Harbor.

(27) Petro, T. M., Schwartzbach, S. D., and Zhang, S. (1999) Smokeless tobacco and nicotine bring about excessive cytokine responses of murine memory T-cells. *Int. J. Immunopharmacol. 21*, 103–114.

(28) Sikdar, N., Mahmud, S. A., Paul, R. R., and Roy, B. (2003) Polymorphism in CYP1A1 and CYP2E1 genes and susceptibility to leukoplakia in Indian tobacco users. *Cancer Lett. 195*, 33–42.

(29) Forkert, P. G. (1997) Conjugation of glutathione with the reactive metabolites of 1,1-dichloroethylene in murine lung and liver. *Microsc. Res. Tech. 36*, 234–242.

(30) Petrulis, J. R., and Bunce, N. J. (2000) Competitive behavior in the interactive toxicology of halogenated aromatic compounds. *J. Biochem. Mol. Toxicol. 14*, 73–81.

(31) Cao, Q., Mak, K. M., and Lieber, C. S. (2005) Cytochrome p450 2E1 primes macrophages to increase TNF-α production in response to lipopolysaccharide. *Am. J. Physiol. Gastrointest. Liver Physiol. 289*, G95–G107.

(32) Roberts, R. A., Ganey, P. E., Ju, C., Kamendulis, L. M., Rusyn, I., and Klaunig, J. E. (2007) Role of the Kupffer cell in mediating hepatic toxicity and carcinogenesis. *Toxicol. Sci. 96*, 2–15.

(33) Dey, A., Jones, J. E., and Nebert, D. W. (1999) Tissue- and cell type-specific expression of cytochrome P450 1A1 and cytochrome P450 1A2 mRNA in the mouse localized in situ hybridization. *Biochem. Pharmacol. 58*, 525–537.

(34) Schaaf, G. J., de Groene, E. M., Maas, R. F., Commandeur, J. N. M., and Fink-Gremmels, J. (2001) Characterization of biotransformation enzyme activities in primary rat proximal tubular cells. *Chem.-Biol. Interact. 134*, 167–190.

(35) Sundberg, A., Appelkvist, E. L., Dallner, G., and Nilsson, R. 1994a Glutathione transferases in the urine: Sensitive methods for detection of kidney damage induced by nephrotoxic agents in humans. *Environ. Health Perspect. 102*, 293–296.

(36) Sundberg, A. G., Appelkvist, E. L., Backman, L., and Dallner, G. 1994b Urinary π-class glutathione transferase as an indicator of tubular damage in the human kidney. *Nephron 67*, 308–316.

(37) Chichester, C. H., Buckpitt, A. R., Chang, A., and Plopper, C. G. (1994) Metabolism and cytotoxicity of naphthalene and its metabolites in isolated murine Clara cells. *Mol. Pharmacol. 45*, 664–672.

(38) Iverson, S. L., Hu, L. Q., Vukomanovic, V., and Bolton, J. L. (1995) The influence of the *p*-alkyl substituent on the isomerization of *o*-quinones to *p*-quinone methides: Potential bioactivation mechanism for catechols. *Chem. Res. Toxicol. 8*, 537–544.

(39) Das, R. K., and Dash, B. C. (1992) Genotoxicity of 'Gudakhu', a tobacco preparation. II. In habitual users. *Food Chem. Toxicol. 30*, 1045–1049.

(40) Kayal, J. J., Trivedi, A. H., Dave, B. J., Nair, J., Nair, U. J., Bhide, S. V., Goswami, U. C., and Adhvaryu, S. G. (1993) Incidence of micronuclei in oral mucosa of users of tobacco products singly or in various combinations. *Mutagenesis 8*, 31–33.

(41) Ozkul, Y., Donmez, H., Erenmemisoglu, A., Demirtas, H., and Imamoglu, N. (1997) Induction of micronuclei by smokeless tobacco on buccal mucosa cells of habitual users. *Mutagenesis 12*, 285–287.

(42) Petruska, J. M., Mosebrook, D. R., Jakob, G. J., and Trush, M. A. (1992) Myeloperoxidase enhanced formation of (+)-trans-7,8-dihydroxy-7,8-dihydrobenzo[a]pyrene-DNA adducts in lung tissue in vitro: A role of pulmonary inflammation in the bioactivation of a procarcinogen. *Carcinogenesis 13*, 1075–1081.

(43) Henderson, J. P., Byun, J., Takeshita, J., and Heinecke, J. W. (2003) Phagocytes produce 5-chlorouracil and 5-bromouracil, two mutagenic products of myeloperoxidase, in human inflammatory tissue. *J. Biol. Chem. 278*, 23522–23528.

(44) Jiang, Q., Blount, B. C., and Ames, B. N. (2003) 5-Chlorouracil, a marker of DNA damage from hypochlorous acid during inflammation. A gas chromatography-mass spectrometry assay. *J. Biol. Chem. 278*, 32834–32840.

(45) Tan, M., Li, S., Swaroop, M., Guan, K., Oberley, L. W., and Sun, Y. (1999) Transcriptional activation of the human glutathione peroxidase promoter by p53. *J. Biol. Chem. 274*, 12061–12066.

(46) Polyak, K., Waldman, T., He, T. C., Kinzler, K. W., and Vogelstein, B. (1996) Genetic determinants of p53-induced apoptosis and growth arrest. *Genes Dev. 10*, 1945–1952.

(47) Liebmann, J., Fisher, J., Lipschultz, C., Kuno, R., and Kaufman, D. C. (1995) Enhanced glutathione peroxidase expression protects cells from hydroperoxides but not from radiation or doxorubicin. *Cancer Res. 55*, 4465–4470.

(48) Kayanoki, Y., Fujii, J., Islam, K. N., Suzuki, K., Kawata, S., Matsuzawa, Y., and Taniguchi, N. (1996) The protective role of glutathione peroxidase in apoptosis induced by reactive oxygen species. *J. Biochem. 119*, 817–822.

(49) Miyashita, T., Krajewski, S., Krajeweska, M., Wang, H. G., Lin, H. K., Liebermann, D. A., Hoffman, B., and Reed, J. C. (1994) Tumor suppressor p53 is a regulator of bcl2 and bax expression in vitro and in vivo. *Oncogene 9*, 1799–1805.

(50) Miyashita, T., and Reed, J. C. (1995) Tumor suppressor p53 is a direct transcriptional activator of the human Bax gene. *Cell 80*, 293–299.

(51) Selvakumaran, M., Lin, H. K., Miyashita, T., Wang, H. G., Krajewski, S., Reed, J. C., Hoffman, B., and Liebermann, D. (1994) Immediately early upregulation of bax expression by p53 but not TGFb1: A paradigm for distinct apoptotic pathways. *Oncogene 9*, 1791–1798.

(52) Zhan, Q., Bae, I., Kastan, M. B., and Fornace, A. J., Jr. (1994) The p53-dependent gamma-ray response of GADD45. *Cancer Res. 54*, 2755–2760.

(53) Brady, H. J., Salomons, G. S., Bobeldijk, R. C., and Berns, A. J. (1996) T-cells from bax-alpha transgenic mice show accelerated apoptosis in response to stimuli but do not show restored DNA damage induced cell death in the absence of p53. *EMBO J. 15*, 1221–1230.

(54) Agusti, A. G., and Rodriguez-Roisin, R. (1993) Effect of pulmonary hypertension on gas exchange. *Eur. Respir. J. 6*, 1371–1377.

(55) Tomita, Y., Bilim, V., Kawasaki, T., Takahashi, K., Okan, I., Magnusson, K. P., and Wiman, K. G. (1996) Frequent expression of Bcl-2 in renal-cell carcinomas carrying wild-type p53. *Int. J. Cancer 66*, 322–325.

(56) Budhram-Mahadeo, V., Morris, P. J., Smith, M. D., Midgley, C. A., Boxer, L. M., and Latchman, D. S. (1999) p53 suppresses the activation of the Bcl-2 promoter by the Brn-3a POU family transcription factor. *J. Biol. Chem. 274*, 15237–15244.

TX900458X